SLAC-PUB-12852
arXiv:0709.4294[astro-ph]
October 2007

New constraints on dark energy from the observed growth of the most X-ray luminous galaxy clusters

A. Mantz,[1⋆] S. W. Allen,[1] H. Ebeling[2] and D. Rapetti[1]
[1] *Kavli Institute for Particle Astrophysics and Cosmology, Stanford University, 382 Via Pueblo Mall, Stanford, CA 94305-4060, USA*
[2] *Institute for Astronomy, 2680 Woodlawn Drive, Honolulu, HI 96822, USA*

26 September 2007

ABSTRACT

We present constraints on the mean matter density, $\Omega_{\rm m}$, normalization of the density fluctuation power spectrum, σ_8, and dark energy equation of state parameter, w, obtained from the X-ray luminosity function of the Massive Cluster Survey (MACS) in combination with the local BCS and REFLEX galaxy cluster samples. Our analysis incorporates the mass function predictions of Jenkins et al. (2001), a mass–luminosity relation calibrated using the data of Reiprich and Böhringer (2002), and standard priors on the Hubble constant, H_0, and mean baryon density, $\Omega_{\rm b}h^2$. We find $\Omega_{\rm m} = 0.27^{+0.06}_{-0.05}$ and $\sigma_8 = 0.77^{+0.07}_{-0.06}$ for a spatially flat, cosmological constant model, and $\Omega_{\rm m} = 0.28^{+0.08}_{-0.06}$, $\sigma_8 = 0.75 \pm 0.08$ and $w = -0.97^{+0.20}_{-0.19}$ for a flat, constant-w model (marginalized 68 per cent confidence intervals). Our findings constitute the first precise determination of the dark energy equation of state from measurements of the growth of cosmic structure in galaxy clusters. The consistency of our result with $w = -1$ lends strong additional support to the cosmological constant model. The constraints are insensitive to uncertainties at the 10–20 per cent level in the mass function and in the redshift evolution of the mass–luminosity relation; the constraint on dark energy is additionally robust against our choice of priors and known X-ray observational biases affecting the mass–luminosity relation. Our results compare favorably with those from recent analyses of type Ia supernovae, cosmic microwave background anisotropies, the X-ray gas mass fraction of relaxed galaxy clusters and cosmic shear. A simplified combination of the luminosity function data with supernova, cosmic microwave background and cluster gas fraction data using importance sampling yields the improved constraints $\Omega_{\rm m} = 0.263 \pm 0.014$, $\sigma_8 = 0.79 \pm 0.02$ and $w = -1.00 \pm 0.05$.

Key words: cosmological parameters – large-scale structure of Universe – X-rays: galaxies: clusters.

1 INTRODUCTION

In the hierarchical collapse scenario for structure formation in the universe, the number density of collapsed objects as a function of mass and cosmic time is a sensitive probe of cosmology. The galaxy clusters that occupy the high-mass tail of this population provide a powerful and relatively clean tool for cosmology, since their growth is predominantly determined by linear gravitational processes. In the past, the local population of galaxy clusters has been used to constrain the average matter density of the universe and the amplitude of perturbations in the density field (e.g. Reiprich & Böhringer 2002; Seljak 2002; Viana et al. 2002; Allen et al. 2003; Pierpaoli et al. 2003; Schuecker et al. 2003; Voevodkin & Vikhlinin 2004; Dahle 2006; Rozo et al. 2007). Pushing observations to higher redshift breaks the degeneracy between those two parameters (e.g. Donahue & Voit 1999; Eke et al. 1998; Henry 2000; Borgani et al. 2001; Vikhlinin et al. 2003), and allows properties of dark energy to be probed as well (e.g. Haiman et al. 2001; Levine et al. 2002; Weller et al. 2002; Majumdar & Mohr 2003, 2004; Henry 2004).

Investigations of this type require sky surveys with well understood selection functions to find clusters, as well as a relation linking cluster mass with an observable. A successful solution to the former requirement has been to identify clusters by the X-ray emission produced by hot intracluster gas, notably using data from the *ROSAT* All-Sky Survey (RASS; Trümper 1993). The *ROSAT* Brightest Cluster Sample (BCS; Ebeling et al. 1998, 2000) and *ROSAT*-ESO Flux Limited X-ray sample (REFLEX; Böhringer et al. 2004) together cover approximately two-thirds of the sky out

⋆ E-mail: amantz@stanford.edu

Submitted to Monthly Notices of the Royal Astronomical Society
Work supported in part by US Department of Energy contract DE-AC02-76SF00515

to redshift $z \sim 0.3$ and contain more than 750 clusters. The Massive Cluster Survey (MACS; Ebeling et al. 2001, 2007) – which at this writing contains 126 clusters and covers 55 per cent of the sky – aims to extend these data to $z \sim 0.7$.

The most straightforward mass–observable relation to complement an X-ray flux-limited survey is the mass–X-ray luminosity relation. It has the advantages that luminosities can be estimated directly from the survey data, and that the selection function is identical to the requirement for detectability of the survey. Thus, every cluster in a flux complete survey can be used in the analysis, without the need for additional observations other than those required to calibrate the mass–luminosity relation. A disadvantage is that there is a large scatter in cluster luminosities at fixed mass; however, sufficient data allow this scatter to be quantified empirically. Alternative approaches use cluster temperature (Henry 2000; Seljak 2002; Pierpaoli et al. 2003; Henry 2004), gas fraction (Voevodkin & Vikhlinin 2004) or Y_X parameter (Kravtsov et al. 2006) to achieve tighter mass–observable relations at the expense of greatly reducing the size of the samples available for analysis. The need to quantify the selection function in terms of both X-ray flux and a second observable additionally complicates these efforts.

In this paper, we use the observed X-ray luminosity function to investigate two cosmological scenarios, assuming a spatially flat metric in both cases: the first includes dark energy in the form of a cosmological constant (ΛCDM); the second has a spatially uniform dark energy component for which density evolves according to a fixed equation of state parameter, w (wCDM). In each case, our results are in good agreement with findings from independent cosmological data sets, notably type Ia supernovae (SNIa), the cosmic microwave background (CMB), the X-ray gas mass fraction of galaxy clusters ($f_{\rm gas}$), and measurements of cosmic shear. For the wCDM model, we obtain $w = -0.97^{+0.20}_{-0.19}$, consistent with a cosmological constant.

Unless otherwise noted, specific masses and luminosities quoted in this paper or shown in figures are computed with respect to a spatially flat ΛCDM reference cosmology with $h = H_0/100\,{\rm km\,s^{-1}\,Mpc^{-1}} = 0.7$ and $\Omega_{\rm m} = 0.3$. Luminosities and fluxes refer specifically to the 0.1–2.4 keV energy band in the source and observer rest frames, respectively. We will consistently use the notation L to denote to the true luminosity of a cluster and $\hat{L}$ to denote the luminosity inferred from observation. We will also write, for example, $\Omega_{\rm m}$ to refer to the present day matter density in units of the critical density, whereas $\Omega_{\rm m}(z)$ is the same quantity at redshift z.

2 THEORY

The variance of the linearly evolved density field, smoothed by a spherical top-hat window of comoving radius R, enclosing mass $M = 4\pi\bar{\rho}_m R^3/3$, is

$$\sigma^2(M,z) = \frac{D^2(z)}{2\pi^2}\int_0^\infty k^2 P(k)|W_M(k)|^2 dk. \quad (1)$$

Here $\bar{\rho}_m$ is the mean comoving matter density of the universe, $P(k)$ is the linear power spectrum at redshift zero, $W_M(k)$ is the Fourier transform of the window function, and $D(z) = \sigma_8(z)/\sigma_8(0)$ is the growth factor of linear perturbations, normalized to unity at $z = 0$. The power spectrum, $P(k) \propto k^{n_s}T^2(k)$, can be evaluated using, for example, the transfer function $T(k)$ of Eisenstein & Hu (1998).[1] The growth factor is

$$D(z) = \frac{g(z)}{g(0)}\frac{1}{1+z}, \quad (2)$$

where, for the wCDM cosmology, $g(z)$ satisfies the second order differential equation (Linder 2005)

$$g'' + \left[\frac{5}{2} - \frac{3}{2}w\Omega_w(a)\right]g' + \frac{3}{2}(1-w)\Omega_w(a)g = 0. \quad (3)$$

Here the derivatives are with respect to $\ln(a)$ and Ω_w denotes the dark energy density. The corresponding equation for ΛCDM is simply obtained by setting $w = -1$.

Jenkins et al. (2001, hereafter J01) and Evrard et al. (2002) have shown that the predicted mass function of galaxy clusters of mass M at redshift z can be written in terms of a "universal" function of $\sigma^{-1}(M,z)$,

$$f(\sigma^{-1}) = \frac{M}{\bar{\rho}_m}\frac{dn(M,z)}{d\ln\sigma^{-1}}, \quad (4)$$

which can be fit by a simple form,

$$f(\sigma^{-1}) = A\exp\left(-|\ln\sigma^{-1} + B|^\epsilon\right), \quad (5)$$

for cosmological constant models. It has since been verified that this fitting function is approximately universal among models with constant $w \neq -1$ and some evolving-w models (Klypin et al. 2003; Linder & Jenkins 2003; Łokas et al. 2004). We adopt the values $A = 0.316$, $B = 0.67$ and $\epsilon = 3.82$ from J01, determined using a spherical overdensity group finder at an overdensity of 324 times the mean matter density ($324m$). The number density per unit mass of galaxy clusters of mass M at redshift z is then

$$\frac{dn(M,z)}{dM} = \frac{\bar{\rho}_m}{M}\frac{d\ln\sigma^{-1}}{dM}f(\sigma^{-1}). \quad (6)$$

Following Morandi et al. (2007), we describe the relationship between mass and X-ray luminosity for massive clusters as self-similar (e.g. Bryan & Norman 1998), modified by an additional redshift-dependent factor

$$E(z)M = M_0(1+z)^\gamma\left(\frac{L}{E(z)}\right)^\beta, \quad (7)$$

where $E(z) = H(z)/H_0$. Our model also includes a log-normal scatter of width η in luminosity for a given mass.

For comparability with the Jenkins mass function, this relation must use a consistent definition of cluster mass (*i.e.* M_{324m}). As there is no universal convention among observers for the overdensity used to define mass, it is necessary to convert masses obtained from the literature to the appropriate overdensity (White 2002). Details of carrying out this conversion, assuming a spherically symmetric Navarro, Frenk, & White (1997) density profile, are reviewed in Hu & Kravtsov (2003).[2]

[1] We employ their "effective shape" function, which includes baryon suppression but not oscillations.

[2] We assume a concentration parameter $c = 5.0$ when making this conversion.

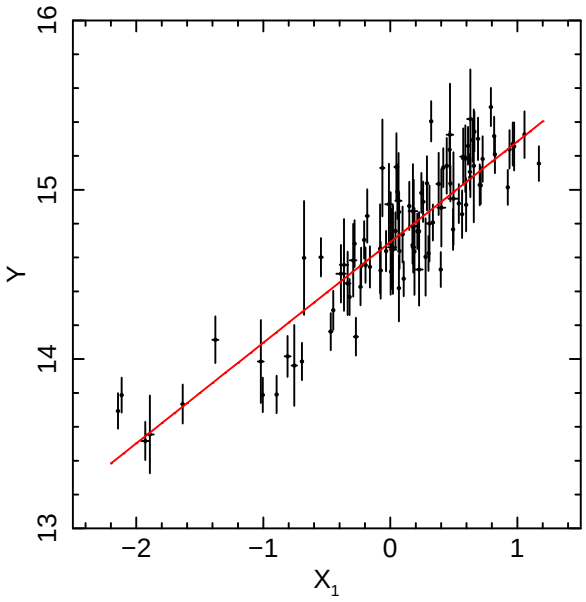

Figure 1. Mass–luminosity data of RB02 and the best-fitting relation (Equation 8). The quantities Y and X_1 are defined in Equation 9. As noted in the text, we have excluded the 6 clusters at $z > 0.11$ from the complete RB02 sample. The masses and luminosities are computed for our reference cosmology; the masses correspond to a spherical overdensity of 324 with respect to $\bar{\rho}_m$, matching the Jenkins mass function.

Equations 6 and 7, combined with a suitable stochastic model linking the true luminosity of a cluster with its observed flux, provide the means to predict the galaxy cluster luminosity function based on a set of model parameters. The procedure used to constrain these parameters is described in Section 4.

3 OBSERVATIONS

3.1 Mass–luminosity relation

3.1.1 X-ray data

We have determined the mass–luminosity relation of galaxy clusters using the sample of Reiprich & Böhringer (2002, hereafter RB02), shown in Fig. 1. In these data, the luminosities were measured from a combination of pointed *ROSAT* PSPC and RASS data. The masses within r_{500} (M_{500}) were determined by fitting the surface brightness profile with a β-model (Cavaliere & Fusco-Femiano 1978) and applying the hydrostatic equation, assuming that the intracluster gas is isothermal. Here r_{500} is the radius within which the mean density is 500 times the critical density, ρ_c, not the universal mean matter density, $\bar{\rho}_m$.

The assumption of hydrostatic equilibrium introduces a bias into the derived mass due to the presence of non-thermal support and asphericity in the observed clusters (Faltenbacher et al. 2005; Rasia et al. 2006). We attempt to correct for this bias using the results of Nagai et al. (2007), who find that the hydrostatic mass determinations of simulated clusters at $z = 0$ systematically underestimate M_{500} by 25.3 ± 16.2 per cent. This figure is an average over simulated clusters in both relaxed and unrelaxed states, and additionally takes into account the observational bias in the determination of r_{500}.

We fit the log-linear model (see Equation 7)

$$Y = \alpha + \beta X_1 + \gamma X_2, \tag{8}$$

where

$$\begin{aligned} Y &= \log_{10}\left(\frac{E(z)M_{324m}}{\mathrm{M}_\odot}\right) \\ X_1 &= \log_{10}\left(\frac{L}{E(z)10^{44}\,\mathrm{erg\,s^{-1}}}\right) \\ X_2 &= \log_{10}(1+z) \\ \alpha &= \log_{10}\left(\frac{M_0}{\mathrm{M}_\odot}\right). \end{aligned} \tag{9}$$

The process of fitting this model is potentially complicated by the presence of Malmquist bias. Close to the flux limit for selection, any X-ray selected sample will preferentially include the most luminous sources for a given mass. This results in a steepening of the derived mass–luminosity relation and a bias in the inferred intrinsic scatter in luminosity for a given mass. (The inferred intrinsic dispersion may be artificially reduced or increased, depending on the distribution of data with respect to the flux limit.) The inclusion of the full sample of RB02, rather than only their flux-limited HIFLUGCS sample, partially mitigates this effect by softening the flux limit. Furthermore, we eliminate the 6 clusters at redshifts > 0.11 which all lie close the the flux limit; as Fig. 2 shows, the extent in luminosity of the remaining 100 clusters is roughly a decade at all redshifts. As our estimate (see below) of the intrinsic scatter in X_1 is roughly 0.17 (*i.e.* 0.17 decades in luminosity), and the Poisson measurement error is much smaller, we expect the effects of Malmquist bias on our estimation of the power-law slope and intrinsic dispersion to be minimal.

A second consequence of Malmquist bias is that there is a strong apparent, but not necessarily physical, correlation between luminosity and redshift due to the fact that the flux limit corresponds to higher luminosities at higher redshifts. (This is evident in Fig. 2.) Within redshift 0.11, we expect this false signal to be much greater than any real evolution; we therefore fix $\gamma = 0$ when fitting the model.

Although methods exist for performing linear regression on data with bivariate heteroscedastic errors and intrinsic scatter (e.g. Akritas & Bershady 1996), such methods do not provide a simple goodness-of-fit measure that can be associated with arbitrary values of the fit parameters. In contrast, the χ^2 statistic is an easily calculated measure of goodness-of-fit, but is biased by the presence of intrinsic scatter. We compromise by using a modified χ^2 which accounts for intrinsic scatter by introducing an additional dispersion term,

$$\tilde{\chi}^2 = \sum_j \frac{(\alpha + \beta X_{1,j} - Y_j)^2}{\varepsilon_{Y,j}^2 + \Delta}, \tag{10}$$

where $\varepsilon_{Y,j}$ is the measurement error on Y_j and Δ is the additional dispersion. This statistic is defined in terms of Y given X_1 because the luminosity measurement errors are negligible in comparison to the mass measurement errors (Fig. 1). The value of Δ is chosen iteratively, adjusting it such that the best fit, found by minimizing $\tilde{\chi}^2$ using least-squares methods, has $\tilde{\chi}^2$ equal to the median of the chi-

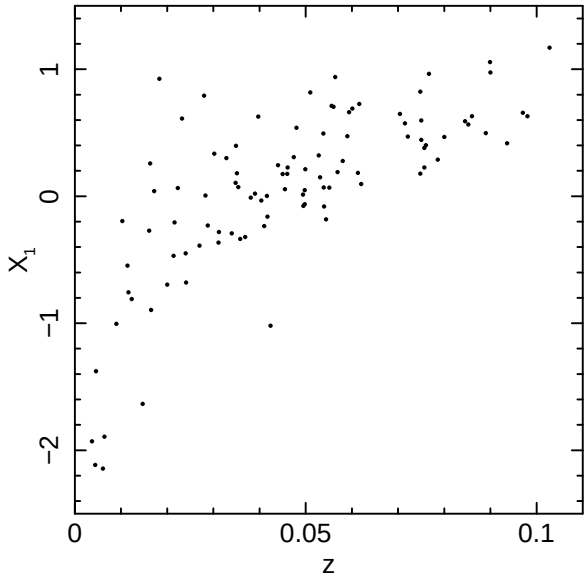

Figure 2. Luminosity–redshift distribution of the RB02 data. The quantity X_1 is defined in Equation 9 and is computed in our reference cosmology. As noted in the text, we have excluded the 6 clusters at $z > 0.11$ from the complete RB02 sample. The remaining clusters have an extent of roughly one decade in luminosity at all redshifts.

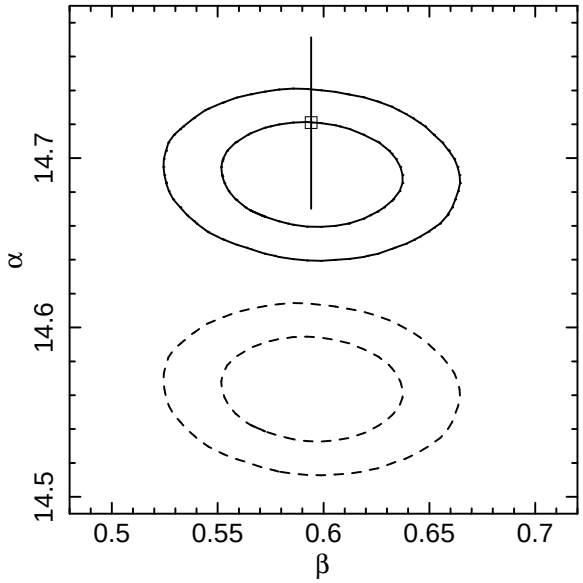

Figure 3. 68.3 and 95.4 per cent confidence regions for the mass–luminosity parameters α and β from the RB02 data (solid lines). Also shown is the best fit and 68.3 per cent confidence interval (square with error bars) on α with fixed β obtained from the Dahle (2006) data (Section 3.1.2). The cosmology is fixed at our reference. The dashed lines are the confidence regions that would been obtained from the RB02 data if the the masses were not corrected for bias due to the assumption of hydrostatic equilibrium.

square distribution with $\nu = 100 - 2$ degrees of freedom (*i.e.* $\tilde{\chi}^2/\nu \approx 1$). The $\tilde{\chi}^2$ statistic thus does not measure absolute goodness-of-fit, but goodness relative to the best fit. Note that in the cosmological analysis (Section 4.1) we use a fixed value of Δ rather than repeating this iterative process for each step in the Markov chain.

The log-normal intrinsic dispersion in luminosity for a given mass can be estimated from the scatter in the data about the best fit, with measurement errors subtracted in quadrature,

$$\hat{\eta}^2 = \frac{1}{\nu}\sum_j \left[\left(\frac{Y_j - \alpha_0}{\beta_0} - X_{1,j} \right)^2 - \varepsilon_{X_1,j}^2 - \left(\frac{\varepsilon_{Y,j}}{\beta_0} \right)^2 \right], \quad (11)$$

where α_0 and β_0 are the parameters describing the best fit. Under assumptions of normal measurement errors and intrinsic scatter, the quantity $\hat{\eta}^2\nu/\eta^2$ is drawn from a chi-square distribution with ν degrees of freedom. It follows that the likelihood of the observed $\hat{\eta}^2$ given the model parameter η^2 is the same chi-square density multiplied by ν/η^2:

$$P(\hat{\eta}^2|\eta^2) = \frac{\left(\hat{\eta}^2\right)^{\nu/2-1}}{2^{\nu/2}\Gamma(\nu/2)} \left(\frac{\nu}{\eta^2}\right)^{\nu/2} \exp\left(-\frac{\nu\hat{\eta}^2}{2\eta^2}\right). \quad (12)$$

This provides a goodness-of-fit measure for η (see Section 4.1).

Confidence regions for α and β obtained with cosmological parameters fixed at our reference and using uniform priors on α, β and η are displayed as in Fig. 3 (solid lines). The best-fitting values and marginal 68.3 per cent confidence intervals are $\alpha = 14.69 \pm 0.02$, $\beta = 0.59 \pm 0.03$ and $\eta = 0.165 \pm 0.012$. Our results for the slope and intrinsic scatter of the relation are in good agreement with the original conclusions of RB02, obtained using bootstrap monte carlo with the BCES estimator of Akritas & Bershady (1996). A quantile-quantile plot of the residuals in X_1 for the best fit (Fig. 4) confirms that the distribution of luminosities for a given mass is reasonably approximated by the log-normal distribution.

3.1.2 Weak lensing data

In order to verify the appropriateness of the hydrostatic bias correction applied to the RB02 masses, we compare the results of Section 3.1.1 with the data of Dahle (2006), for which masses were measured using weak gravitational lensing. These masses, with associated luminosities taken from the BCS and extended BCS (eBCS) catalogs, are shown in Fig. 5 (black points). In contrast to the RB02 data, the Malmquist bias due to the (e)BCS flux limit is clearly evident; in particular, the lowest-mass clusters in this data set are very likely to represent the upper tail of the distribution of luminosities for given mass. Although the simple methods described above are unsuitable for fitting the mass–luminosity relation when the data are subject to significant Malmquist bias, the intersection of these two data sets near the highest observed masses indicates that they are compatible.

We can quantify this observation by using the Dahle data to fit for the normalization, α, by minimizing $\tilde{\chi}^2$, while leaving the slope, β, fixed at the best-fitting value from Section 3.1.1. The resulting one-dimensional 68.3 per cent confidence interval on α is shown in Fig. 3. The best-fitting normalization ($\alpha = 14.72$) is well within the 95.4 per cent confidence region obtained using the corrected RB02 data. Without applying the bias correction (~ 0.13 in Y) to the X-ray determined masses it would fall well beyond the allowed region (dashed lines in Fig. 3). This result confirms observationally both that a correction is needed when masses are

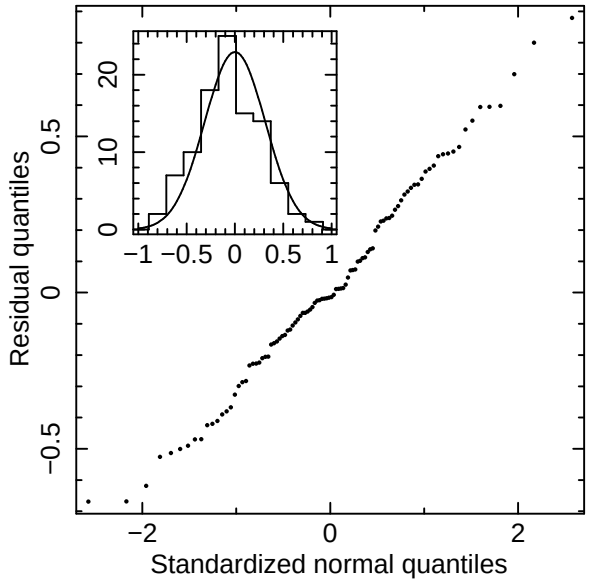

Figure 4. Quantile-quantile plot comparing the residuals in X_1 of the RB02 data for the best fitting relation to a normal distribution. The straightness of the distribution indicates that the scatter is well approximated as normal in X_1 (log-normal in luminosity). Inset: the histogram of X_1 residuals is directly compared with the normal distribution.

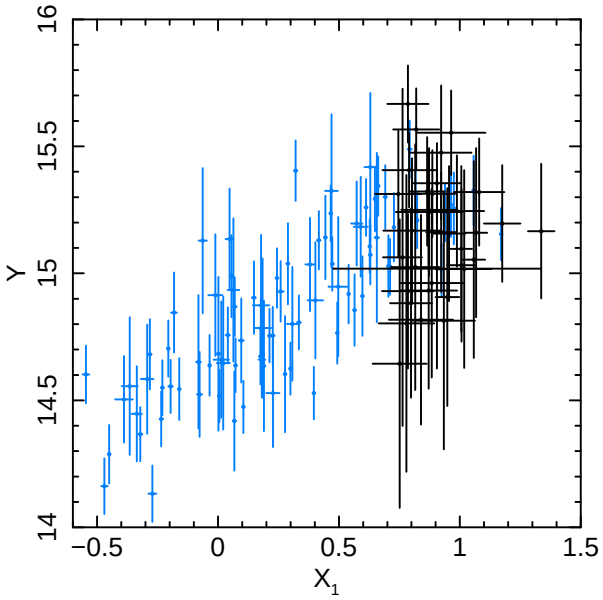

Figure 5. The mass–luminosity data of Dahle (2006) (black) are compared with those of RB02 (blue; see additional comments of Fig. 1). The effect of the (e)BCS flux limit on the Dahle data ($X_1 \sim 0.75$) is clearly evident. At lower masses, the data set is progressively more likely to contain only the most luminous clusters for that mass, resulting in an apparent steepening of the relation.

measured using an X-ray analysis that assumes hydrostatic equilibrium, and that the magnitude of the effect reported by Nagai et al. (2007) is roughly correct.

3.2 X-ray luminosity function

We use three flux-limited surveys in our analysis: the BCS (Ebeling et al. 1998) and REFLEX (Böhringer et al. 2004) at low redshifts ($z < 0.3$), and the MACS (Ebeling et al. 2001) at $0.3 < z < 0.7$. (We restricted the REFLEX sample to the southern hemisphere so that its coverage on the sky would not overlap the BCS.) As discussed in Section 4.2, a proper accounting of the intrinsic scatter in the mass–luminosity relation involves convolving over all possible masses when evaluating the likelihood of a set of cosmological parameters; it is therefore necessary for the mass–luminosity relation to be well calibrated at luminosities significantly (at least an order of magnitude) below those allowed in the surveys. We thus also restrict the analysis to clusters with large inferred luminosities $\hat{L} > 2.55 \times 10^{44} h_{70}^{-2}\,\mathrm{erg\,s^{-1}}$.

The completeness of the REFLEX sample has been investigated by Böhringer et al. (2001) and Schuecker et al. (2001), and is thought to be well above 90 per cent at a flux limit of $3.0 \times 10^{-12}\,\mathrm{erg\,s^{-1}\,cm^{-2}}$. The BCS completeness as a function of flux is quantified in Ebeling et al. (1998); we use a flux limit of $4.4 \times 10^{-12}\,\mathrm{erg\,s^{-1}\,cm^{-2}}$ where the BCS completeness is 90 per cent. Most of the incompleteness in the BCS is due to the inefficient extended-source detection of the RASS II algorithm, which is most severe at very low redshifts. One consequence of our high luminosity cut is that the sample contains mostly higher redshift objects ($\bar{z} \approx 0.21$) and not the large number of low redshift, low luminosity objects that would be included in a strictly flux-limited sample. The reported completeness of the BCS is thus an underestimate for the subsample of very luminous clusters used in our analysis. We have repeated the analysis of the BCS data alone (see Section 5.1) using a higher flux limit ($5 \times 10^{-12}\,\mathrm{erg\,s^{-1}\,cm^{-2}}$) where the reported BCS incompleteness is negligible, and obtain a similar result. We conclude that significant incompleteness is not present in the BCS, given our selection criteria. The similar number of clusters (78 and 80, respectively) in the BCS and REFLEX samples satisfying the BCS flux limit and our luminosity cut support this conclusion.

Unlike the BCS and REFLEX, for which extended-source fluxes were measured using the Voronoi tessellation and percolation (Ebeling 1993; Ebeling & Wiedenmann 1993) and growth curve analysis (Böhringer et al. 2000) algorithms, respectively, reported MACS fluxes are measured within a fixed angular size aperture (5 arcmin in most cases). A redshift-dependent correction for missing flux, described in Ebeling et al. (2001), is required when converting this aperture flux to total flux, both when determining luminosities for the detected clusters themselves and when computing the aperture flux-dependent survey sky coverage (Ebeling et al. 2007). We adopt an aperture flux limit of $2 \times 10^{-12}\,\mathrm{erg\,s^{-1}\,cm^{-2}}$ for MACS, corresponding to the flux above which the optical follow-up of cluster candidates is complete as of this writing. We assess the completeness of this subsample by comparing the MACS $\log N - \log S$ distribution (the number of clusters exceeding aperture flux S as a function of S) to predictions based on cosmologies that are consistent with the BCS+REFLEX data (see Sec-

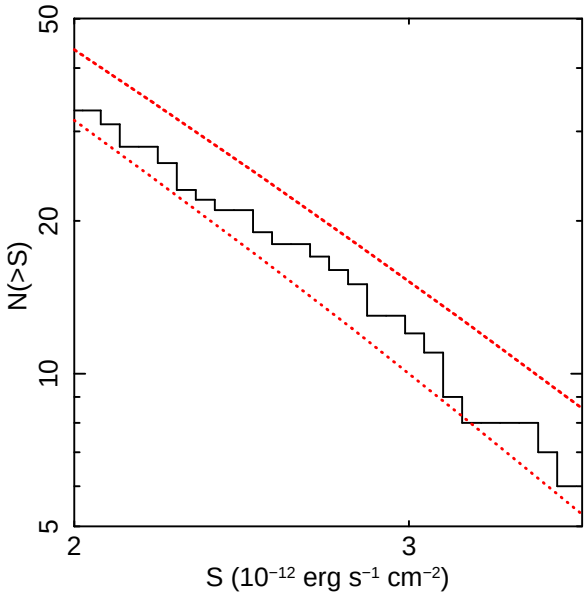

Figure 6. Number of MACS clusters exceeding flux S as a function of S ($\log N - \log S$ distribution). Here S is the flux measured within a 5 arcmin aperture (see text). Dotted red lines are the 68.3 per cent confidence bounds on the $\log N - \log S$ distribution predicted by cosmologies that are consistent with the BCS+REFLEX data, whose completeness has been independently verified. The good agreement between the observed and predicted number of clusters demonstrates that the completeness of the sample is high.

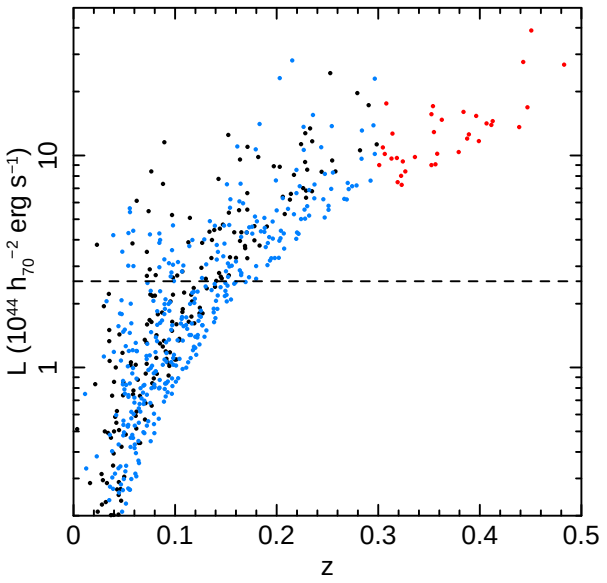

Figure 7. Luminosity–redshift distribution of clusters in the BCS (black), REFLEX (blue) and MACS (red) which are above the respective flux limits (see text). The adopted minimum luminosity of $2.55 \times 10^{44} h_{70}^{-2}\,\mathrm{erg\,s^{-1}}$ is indicated by the dashed line. Error bars are not shown. Note that the redshift range covered by MACS extends to $z = 0.7$ even though no clusters above our adopted flux limit were found at $z > 0.5$.

tion 5.1).[3] The agreement, shown in Fig. 6, demonstrates that the sample is statistically complete at the ~ 90 per cent level.

Using the flux limits and luminosity cut described above, the BCS, REFLEX and MACS surveys respectively contribute 78, 130 and 34 clusters to our sample. The luminosity–redshift distribution of these data is displayed in Fig. 7.

In order to adequately take the effects of Eddington bias into account when predicting the number of clusters above our flux and luminosity thresholds for a given cosmology and mass–luminosity relation, we must be able to assign a probability to the luminosity observed from a cluster, given its true luminosity. Ultimately, the distribution is related to a Poisson distribution in the number of photons detected; however, the nontrivial conversion from photon count rate to unabsorbed flux and the variation in exposure times over the sky make the solution from first principles computationally difficult. Instead, we simplify the problem by assuming that the distribution $P(\hat{L}|L)$, where $\hat{L}$ and L are the observed and true luminosities, is normal with mean L. The variance is a function of the observed flux, which we estimate empirically by fitting the flux errors versus flux for the different surveys to a power-law model. We find power-law slopes of 0.52 for the BCS and REFLEX and 0.56 for MACS, consistent with approximately Poisson scaling.

3.3 Other data

In this paper, we first present an analysis based only on the above data along with the priors described in Section 4. We also show results obtained from other cosmological data for comparison purposes in Section 5, and use the luminosity function data to importance sample these independent results in Section 5.2.3. A modified version of the COSMOMC code[4] of Lewis & Bridle (2002, see also Rapetti et al. 2005, 2007) is used to analyze these independent data. The SNIa and $f_{\rm gas}$ results shown are identical to those in Allen et al. (2007). The $f_{\rm gas}$ data are reported in that work and the SNIa results are derived from the compilation of Davis et al. (2007), which includes results from the ESSENCE survey (60 targets; Wood-Vasey et al. 2007; Miknaitis et al. 2007), the SNLS first year data (57 targets; Astier et al. 2006), 45 nearby supernovae (Jha et al. 2007) and the 30 high-redshift supernovae discovered by HST and reported by Riess et al. (2007) for which a 'gold' rating was awarded (192 SNIa in total). Our analysis of the cosmic microwave background (CMB) anisotropies uses three-year Wilkinson Microwave Anisotropy Probe (WMAP) data, including marginalization over a plausible range in the amplitude of the Sunyaev-Z'eldovich signal ($0 < A_{\rm SZ} < 2$) (Spergel et al. 2007). We use the October 2006 version of the WMAP likelihood code.[5]

The model fitted to the CMB data is slightly different

[3] Predictions shown in Fig. 6 are from ΛCDM cosmologies, since the BCS and REFLEX data are too limited in redshift to constrain w. Identical conclusions result from using wCDM models consistent with the BCS and REFLEX data in addition to MACS data at fluxes $> 3.0 \times 10^{-12}\,\mathrm{erg\,s^{-1}\,cm^{-2}}$, where the completeness of the parent RASS Bright Source Catalog has been independently verified (Schuecker et al. 2001).

[4] http://cosmologist.info/cosmomc/

[5] http://lambda.gsfc.nasa.gov/product/map/current/m_sw.cfm

from the one used for the cluster luminosity function. First, we always marginalize over the scalar spectral index, n_s, in the CMB analysis. Since the CMB results are very sensitive to this parameter, this avoids biases that would be introduced by fixing n_s to a particular value. In contrast, the luminosity function constraints are much less sensitive to n_s (Section 5.2.2); the differences in results from the luminosity function when fixing $n_s = 1.0$ versus $n_s = 0.95$ (the WMAP preferred value) are small. Second, when analyzing the CMB data, we include in the model perturbations in the dark energy density which must be present when $w \neq -1$ (Rapetti et al. 2005). These perturbations are not yet incorporated into the model we use for the luminosity function constraints, although we will consider their effect in future work. We note that there is no reason *a priori* to expect that the inclusion of such perturbations affect the luminosity function constraints in the same way that it affects the CMB constraints.

4 ANALYSIS

We parametrize the full model fitted to the X-ray luminosity function data as (h, $\Omega_{\rm b}h^2$, $\Omega_{\rm c}h^2$, σ_8, n_s, w, A, α, β, γ, η), where $\Omega_{\rm c}$ and $\Omega_{\rm b}$ are the cold dark matter and baryon densities ($\Omega_{\rm m} = \Omega_{\rm c} + \Omega_{\rm b}$) and A is the normalization of the Jenkins mass function (Equation 5). In addition to the assumption of spatial flatness, we adopt the Gaussian priors $h = 0.72 \pm 0.08$ (Freedman et al. 2001) and $\Omega_{\rm b}h^2 = 0.0205 \pm 0.0018$ (O'Meara et al. 2001) from the Hubble Key Project and Big Bang nucleosynthesis studies. These latter priors are necessary because the likelihood depends very weakly on h and $\Omega_{\rm b}$, which enter only though the transfer function. We must also place a prior on the mass–luminosity evolution parameter, γ, since it is not constrained by the RB02 data and thus enters the likelihood only through the evaluation of Equation 7. For the standard set of allowances used in this paper, we adopt a uniform prior with the width chosen such that the allowed variation in the normalization of the mass–luminosity relation out to the nominal redshift limit of MACS, $(1+0.7)^\gamma$, is ± 10 per cent. We additionally marginalize over a 10 per cent uncertainty (standard allowance) in the normalization of the J01 mass function, A, based on the residuals of the fitting formula to their simulations over the mass range of interest. For the remaining model parameters (except n_s), uniform priors on the physically allowed domains were used. These priors, used in the determination of the results in Sections 5.1 and 5.2.1, are summarized in Table 1 (labeled "standard" priors). Note that the spectral index is fixed for these results; the effect of marginalizing over n_s is discussed separately in Section 5.2.2. The sensitivity of our results to the choice of priors is analyzed in Section 6.1.

Cosmological constraints were determined via Markov Chain Monte Carlo, employing the Metropolis algorithm. Multiple, randomly-initialized Markov chains were produced for each set of results, and convergence to the posterior distribution was monitored using the Gelman-Rubin criterion, R, which measures the ratio of between-chain to within-chain variances (Gelman & Rubin 1992), as well as by visual inspection. Acceptable convergence was defined by the requirement $R - 1 < 0.05$. The log-likelihood of the data given a set of model parameters is decomposed into the sum $\ell_{\alpha\beta} + \ell_\eta + \ell_{\rm XLF}$, whose terms are described in the remainder of this Section.

Table 1. Priors used in the analysis. All parameters not listed were assigned uniform priors on their physically allowed domains. The standard and weak priors on γ allow a variation of ± 10 and ± 20 per cent in the normalization of the mass–luminosity relation over the redshift range of our data (see text). [a] $N(\mu, \sigma^2)$ indicates the normal distribution with mean μ and variance σ^2, and $U(a, b)$ indicates the uniform distribution with endpoints a and b.

Prior	Parameter	Density[a]	Section
standard	h	$N(0.72, 0.08^2)$	
weak	h	$N(0.72, 0.24^2)$	6.1
standard	$\Omega_{\rm b}h^2$	$N(0.0205, 0.0018^2)$	
weak	$\Omega_{\rm b}h^2$	$N(0.0205, 0.0054^2)$	6.1
standard	n_s	fixed at 1.0	
weak	n_s	$U(0.5, 1.4)$	5.2.2
standard	A	$N(0.316, 0.0316^2)$	
weak	A	$N(0.316, 0.0632^2)$	6.1
standard	γ	$U(-0.20, 0.18)$	
weak	γ	$U(-0.42, 0.34)$	6.1

4.1 Mass–luminosity likelihood

The parameters describing the normalization and slope of the mass–luminosity relation, α and β, are constrained using the $\tilde{\chi}^2$ statistic defined in Equation 10. Only the RB02 data are used. As mentioned previously, we fix the value of Δ to be 0.0186, calculated in our reference cosmology using the method described in Section 3.1.1. This makes values of $\tilde{\chi}^2$ from different steps of the Markov chain directly comparable, while retaining the de-biasing effect of the modification to χ^2.[6] The log-likelihood associated with $\tilde{\chi}^2$ is defined as $\ell_{\alpha\beta} = -\tilde{\chi}^2/2$.

At each step of the chain, the estimated intrinsic dispersion in the mass–luminosity relation, $\hat{\eta}^2$, is computed by Equation 11. The contribution to the log-likelihood from the dispersion is the logarithm of Equation 12,

$$\ell_\eta = \left(\frac{\nu}{2} - 1\right) \ln\left(\hat{\eta}^2\right) + \frac{\nu}{2} \ln\left(\frac{\nu}{2\eta^2}\right) - \frac{\nu\hat{\eta}^2}{2\eta^2}, \qquad (13)$$

where $\nu = 100 - 2$ and the constant term $-\ln\Gamma(\nu/2)$ has been neglected. Intuitively, this term penalizes models for which the intrinsic dispersion is far from the estimated dispersion measured from the RB02 data.

4.2 Luminosity function likelihood

The likelihood that N clusters with inferred luminosities in a range $d\hat{L}$ exist in a volume dV can in general be written as a Poisson probability plus a correction due to the clustering of halos with one another. Given that our sample covers a very wide survey area ($\sim 2/3$ of the sky) and includes only the

[6] The reference cosmology with respect to which $\tilde{\chi}^2$ is defined is unimportant, since the Markov chain is sensitive only to differences in the statistic. In practice, recalculating the value of Δ at each step of the chain results in negligibly small changes in its value.

most luminous, and therefore rare, objects, the clustering term will be negligible compared to the pure Poisson term (e.g. Hu & Kravtsov 2003). If the plane of redshift and inferred luminosity is divided into non-overlapping cells, then the likelihood of our data is simply

$$P\left(\{N_j\}\right) = \prod_j \frac{\tilde{N}_j^{N_j} e^{-\tilde{N}_j}}{N_j!}, \tag{14}$$

where N_j and $\tilde{N}_j$ are the number of clusters detected and predicted in the jth cell, respectively. The log-likelihood is then

$$\ell_{\rm XLF} = \sum_j \left[N_j \ln(\tilde{N}_j) - \tilde{N}_j \right], \tag{15}$$

where the constant term $-\sum_j \ln(N_j!)$ has been dropped.

If the cells are taken to be rectangular, with the jth consisting of the area between redshifts $z_j^{(1)}$ and $z_j^{(2)}$ and inferred luminosities $\hat{L}_j^{(1)}$ and $\hat{L}_j^{(2)}$, then the quantity $\tilde{N}_j$ is

$$\tilde{N}_j = \int_{z_j^{(1)}}^{z_j^{(2)}} dz \frac{dV(z)}{dz} \int_{\hat{L}_j^{(1)}}^{\hat{L}_j^{(2)}} d\hat{L} \frac{d\tilde{n}(z,\hat{L})}{d\hat{L}}, \tag{16}$$

where $V(z)$ is the comoving volume within redshift z. In the absence of intrinsic scatter in the mass–luminosity relation and measurement errors in the observed luminosities, the derivative of the comoving number density would be simply

$$\frac{d\tilde{n}(z,L)}{dL} = f_{\rm sky}(z,L) \frac{dM(L)}{dL} \frac{dn(z,M)}{dM}. \tag{17}$$

Here $f_{\rm sky}$ is the sky coverage fraction of the surveys as a function of redshift and inferred luminosity (*i.e.* flux), dn/dM is the Jenkins mass function (Equation 6) and $M(L)$ is the mass–luminosity relation (Equation 7). The presence of scatter requires us to take into account that a cluster detected with inferred luminosity $\hat{L}$ could potentially have any true luminosity L and mass M, with some associated probability. To calculate the predicted number density correctly, we must therefore convolve with these probability distributions:

$$\begin{aligned} \frac{d\tilde{n}(z,\hat{L})}{d\hat{L}} &= f_{\rm sky}(z,\hat{L}) \int_0^\infty dL\ P(\hat{L}|L) \\ &\quad \times \int_0^\infty dM\ P(L|M) \frac{dn(z,M)}{dM}. \end{aligned} \tag{18}$$

Above, $P(L|M)$ is a log-normal (base 10) distribution whose width is the intrinsic scatter in the mass–luminosity relation, η, and $P(\hat{L}|L)$ is a normal distribution whose width as a function of flux is modeled as a power law, as described in Section 3.2.

The sum over the second term in Equation 15 reduces to the integrated number of predicted clusters in the detection region of the surveys (*i.e.* within the redshift range and above the luminosity and flux thresholds), independent of binning. However, the first term in that equation is dependent on the choice of binning. To make optimal use of the data, the bin size should be taken as small as possible. For sufficiently small bins, the integrals in Equation 16 can be approximated as an integrand multiplied by the constant and cosmologically invariant bin area $\Delta z \Delta\hat{L}/d_L^2$, where d_L is the luminosity distance to the redshift of the bin. The resulting logarithm of this term in Equation 15 may then be neglected, simplifying the log-likelihood to

$$\ell_{\rm XLF} = \sum_i \ln\left(d_L^2 \left.\frac{dV}{dz}\frac{d\tilde{n}}{d\hat{L}}\right|_{z_i,\hat{L}_i} \right) + \int dz d\hat{L} \frac{dV}{dz}\frac{d\tilde{n}}{d\hat{L}}, \tag{19}$$

where the summation is over detected clusters and the integral extends over the detection region of the surveys.

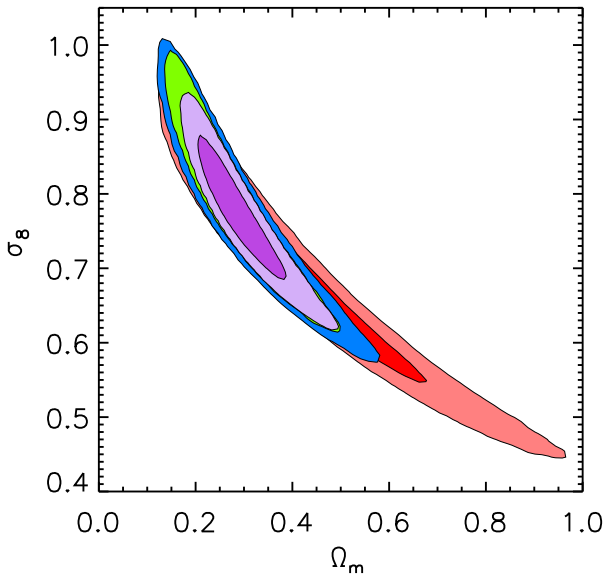

Figure 8. Joint 68.3 and 95.4 per cent confidence constraints on $\Omega_{\rm m}$ and σ_8 for a ΛCDM model from, in order of increasing precision, MACS (red), BCS (blue), and REFLEX (green) individually, and their combination (purple). Note that only the 95.4 per cent confidence regions are visible for the individual BCS and REFLEX data sets. These results assume fixed γ and A (see text), and otherwise use our standard priors (Table 1).

5 RESULTS

5.1 ΛCDM constraints

For a ΛCDM cosmology, any of the X-ray luminosity function (XLF) data sets can individually provide constraints on the model parameters. Fig. 8 shows the joint $\Omega_{\rm m}$-σ_8 constraints obtained from the BCS, REFLEX and MACS data sets individually, as well as their combination. In this figure, we have fixed $\gamma = 0.0$ and $A = 0.316$ in order to emphasize the agreement between the data sets. Using the combined data and standard set of priors (including the marginalizations over γ and A), we obtain $\Omega_{\rm m} = 0.27^{+0.06}_{-0.05}$ and $\sigma_8 = 0.77^{+0.07}_{-0.06}$ (Fig. 9).

These constraints are in good agreement with recent, independent results from the CMB (Spergel et al. 2007) and cosmic shear, as measured in the 100 Square Degree Survey (Benjamin et al. 2007) (Fig. 9). Our results are also in good overall agreement with previous findings based on the observed X-ray luminosity and temperature functions of clusters (e.g. Eke et al. 1998; Donahue & Voit 1999; Henry 2000; Borgani et al. 2001; Seljak 2002; Allen et al. 2003; Pierpaoli et al. 2003; Schuecker et al. 2003; Henry 2004), although the correction to the hydrostatic mass estimates employed in the present study leads to our result on σ_8 being,

Table 2. Best-fitting values and 68.3 per cent confidence intervals for the model parameters obtained from the luminosity function data. Our main results from this study occupy the first three lines; the remaining results are listed in the order that they appear in the text. [a]B=BCS, R=REFLEX, M=MACS. [b]Priors not specified below are standard (see Table 1). 1: all standard; 2: weak n_s prior; 3: fixed $A = 0.316$, $\gamma = 0.0$; 4: fixed A; 5: weak A; 6: fixed A, weak h and $\Omega_b h^2$; 7: fixed A, weak γ; 8: fixed A, $\eta = 0.0$; 9: fixed A, luminosity measurement error= 0.0; 10: fixed A, no correction to RB02 masses.

Data[a]	Model	priors[b]	$\Omega_{\rm m}$	σ_8	w	α	β	η	Section
B+R+M	ΛCDM	1	$0.27^{+0.06}_{-0.05}$	$0.77^{+0.07}_{-0.06}$	—	14.70 ± 0.03	0.60 ± 0.03	0.168 ± 0.012	5.1
B+R+M	wCDM	1	$0.28^{+0.08}_{-0.06}$	0.75 ± 0.08	$-0.97^{+0.20}_{-0.19}$	14.70 ± 0.03	0.60 ± 0.03	$0.165^{+0.014}_{-0.010}$	5.2.1
B+R+M	wCDM	2	$0.23^{+0.17}_{-0.06}$	0.74 ± 0.14	-0.96 ± 0.21	14.69 ± 0.04	0.60 ± 0.03	0.167 ± 0.012	5.2.2
B	ΛCDM	3	0.25 ± 0.08	0.80 ± 0.09	—	14.71 ± 0.04	0.59 ± 0.03	0.167 ± 0.013	5.1
R	ΛCDM	3	$0.24^{+0.08}_{-0.05}$	0.80 ± 0.08	—	14.70 ± 0.03	0.60 ± 0.03	0.164 ± 0.012	5.1
M	ΛCDM	3	$0.30^{+0.20}_{-0.11}$	$0.74^{+0.09}_{-0.13}$	—	14.68 ± 0.05	0.60 ± 0.03	$0.164^{+0.013}_{-0.011}$	5.1
B+R+M	ΛCDM	3	0.27 ± 0.06	0.78 ± 0.06	—	14.70 ± 0.03	0.60 ± 0.03	0.166 ± 0.012	5.1
B+R+M	wCDM	4	$0.27^{+0.09}_{-0.05}$	0.76 ± 0.08	-0.95 ± 0.20	$14.70^{+0.02}_{-0.04}$	0.59 ± 0.03	0.167 ± 0.013	6
B+R+M	wCDM	5	$0.28^{+0.09}_{-0.06}$	0.75 ± 0.08	$-0.96^{+0.20}_{-0.19}$	14.70 ± 0.03	0.60 ± 0.03	$0.166^{+0.14}_{-0.10}$	6.1
B+R+M	wCDM	6	$0.25^{+0.11}_{-0.07}$	$0.74^{+0.15}_{-0.08}$	$-1.02^{+0.26}_{-0.14}$	$14.70^{+0.06}_{-0.05}$	0.60 ± 0.03	$0.165^{+0.015}_{-0.010}$	6.1
B+R+M	wCDM	3	$0.28^{+0.09}_{-0.05}$	0.76 ± 0.08	-0.95 ± 0.18	14.70 ± 0.03	0.60 ± 0.03	$0.169^{+0.010}_{-0.014}$	6.1
B+R+M	wCDM	7	$0.28^{+0.08}_{-0.05}$	$0.75^{+0.08}_{-0.07}$	-0.99 ± 0.23	14.70 ± 0.03	0.59 ± 0.03	0.167 ± 0.012	6.1
B+R+M	wCDM	8	$0.24^{+0.06}_{-0.05}$	0.83 ± 0.08	$-0.99^{+0.20}_{-0.16}$	14.71 ± 0.03	0.60 ± 0.03	—	6.3
B+R+M	wCDM	9	$0.27^{+0.09}_{-0.05}$	0.77 ± 0.08	$-0.91^{+0.17}_{-0.22}$	14.70 ± 0.03	0.60 ± 0.03	0.165 ± 0.012	6.3
B+R+M	wCDM	10	$0.30^{+0.08}_{-0.07}$	0.64 ± 0.07	$-0.99^{+0.22}_{-0.18}$	14.56 ± 0.03	0.60 ± 0.03	0.24 ± 0.02	6.4

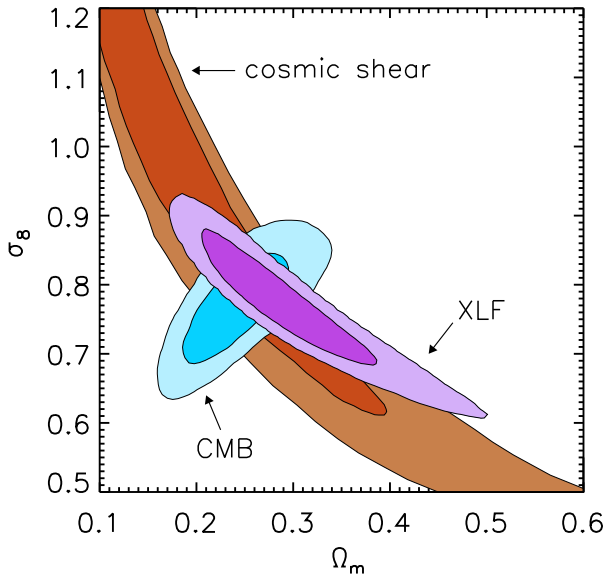

Figure 9. Joint 68.3 and 95.4 per cent confidence constraints on $\Omega_{\rm m}$ and σ_8 for a ΛCDM model using the combined X-ray luminosity function (XLF) data (purple) and our standard priors (Table 1). Also shown are independent constraints from the CMB (blue; Spergel et al. 2007) and cosmic shear (brown; Benjamin et al. 2007)).

typically, somewhat higher (see Section 6.4). Our result on $\Omega_{\rm m}$ is in excellent agreement with current constraints based on cluster $f_{\rm gas}$ data (Allen et al. 2007 and references therein) and the power spectrum of galaxies in the 2dF galaxy redshift survey (Cole et al. 2005) and Sloan Digital Sky Survey (SDSS) (Eisenstein et al. 2005; Tegmark et al. 2006; Percival et al. 2007), as well as the combination of CMB data with a variety of external constraints (Spergel et al. 2007). Our result on σ_8 is marginally lower than that determined by weak lensing tomography in the Cosmic Evolution Survey (COSMOS; Massey et al. 2007) and by the observed number density of optically-selected groups and clusters in the 2dF (Eke et al. 2006) and SDSS surveys (Rozo et al. 2007).

5.2 wCDM constraints

5.2.1 Results using standard priors

In this Section, we investigate the constraints on a constant dark energy equation of state provided by the luminosity function data. Fig. 10 shows the joint constraint on $\Omega_{\rm m}$ and w using our standard priors (purple contours), along with those obtained independently from SNIa (green), CMB data (blue), and cluster $f_{\rm gas}$ data (red). Our results are consistent with each of these independent data, and with the cosmological constant model ($w = -1$). The marginalized results from the luminosity function data are $\Omega_{\rm m} = 0.28^{+0.08}_{-0.06}$, $\sigma_8 = 0.75 \pm 0.08$ and $w = -0.97^{+0.20}_{-0.19}$.

5.2.2 Results marginalized over n_s

We now consider the effect on our constraints of marginalizing over the spectral index n_s. The data are able to constrain the spectral index, although only weakly; in order to speed convergence we impose a uniform prior $0.5 \leqslant n_s \leqslant 1.4$. This prior is still very conservative, given the constraint of the WMAP three-year data, $n_s = 0.951^{+0.015}_{-0.019}$ (Spergel et al. 2007). Fig. 11 shows the joint constraints from our data on $\Omega_{\rm m}$ and σ_8 using standard priors (purple; $n_s = 1.0$) versus this weak uniform prior (gray). The marginalization over n_s has the effect of expanding the constraints along the well-known degeneracy between $\Omega_{\rm m}$ and σ_8; a similar degeneracy is evident in the CMB results (blue, no prior on n_s used).

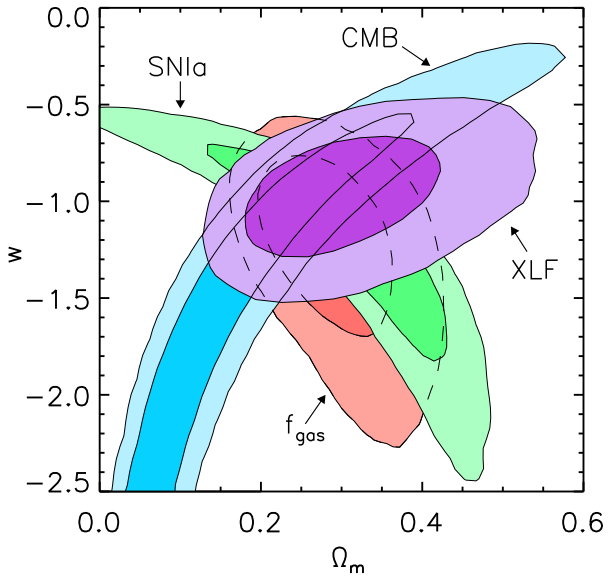

Figure 10. Joint 68.3 and 95.4 per cent confidence constraints on $\Omega_{\rm m}$ and w for a constant-w model using the luminosity function data (purple) and our standard priors (Table 1). Also shown are independent constraints from CMB data (blue; Spergel et al. 2007), SNIa (green; Davis et al. 2007) and cluster $f_{\rm gas}$ data (red; Allen et al. 2007).

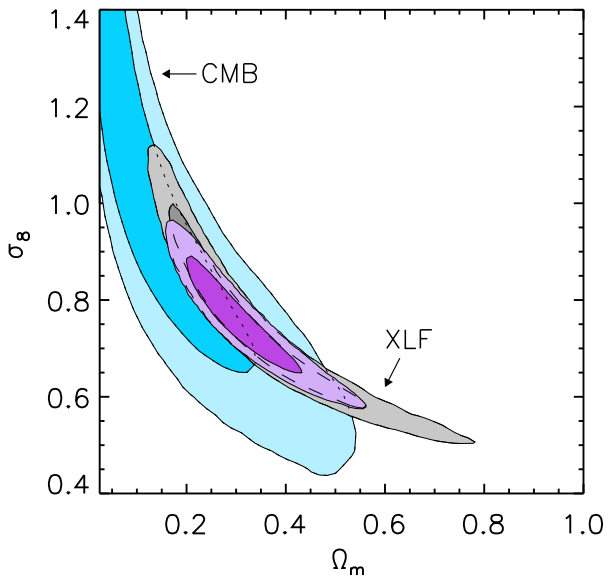

Figure 11. Joint 68.3 and 95.4 per cent confidence constraints on $\Omega_{\rm m}$ and σ_8 for a constant-w model using standard priors (purple; $n_s = 1.0$) and marginalized over n_s (gray). The latter results are in good agreement with independent constraints from the CMB (blue Spergel et al. 2007), also marginalized over n_s.

In contrast, there is no strong degeneracy between n_s and w, and the w constraint is not significantly affected by the marginalization.

5.2.3 Combination with $f_{\rm gas}$+CMB+SNIa data

A detailed analysis of the constraints that can be obtained from a combination of the different cosmological data sets

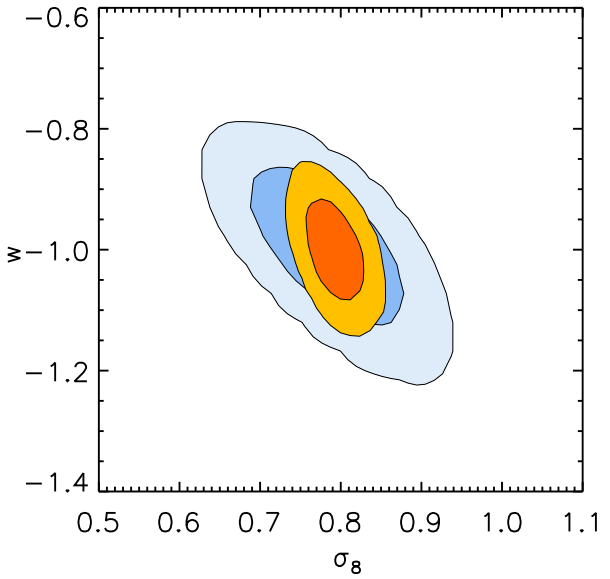

Figure 12. The joint constraints (68.3 and 95.4 per cent confidence) on σ_8 and w obtained from a combined SNIa+$f_{\rm gas}$+CMB analysis (blue) and the improved constraints obtained by combining this with the XLF results using importance sampling (gold). No priors on h, $\Omega_{\rm b}h^2$ or n_s are imposed in either analysis.

is beyond the scope of this paper. Nevertheless, we present here constraints on $\Omega_{\rm m}$, σ_8 and w obtained by using our X-ray luminosity function constraints to importance sample the results of a combined $f_{\rm gas}$+CMB+SNIa analysis (following Allen et al. 2007). Priors on h, $\Omega_{\rm b}h^2$ and n_s are not required or used in this analysis. We note that the wCDM model is treated inconsistently here, in that dark energy perturbations are taken into account in the CMB analysis but not in the XLF analysis; therefore, these results should be interpreted only as a preview of more rigorous future work.

The importance sampling was accomplished by thinning a Markov chain produced from the combined $f_{\rm gas}$+CMB+SNIa analysis and weighting each entry in this thinned chain by the likelihood of the mass–luminosity and luminosity function data (Section 4). This likelihood must be marginalized over all the parameters not addressed by the $f_{\rm gas}$+CMB+SNIa data, namely the mass function normalization, A, and the parameters describing the mass–luminosity relation, α, β, γ and η. However, the posteriors obtained from the luminosity function analysis alone indicate that A and γ are essentially independent of the other parameters; we therefore fixed them at their best-fitting values. The remaining marginalization over α, β and η, was carried out numerically.

The importance-sampled XLF+$f_{\rm gas}$+CMB+SNIa results are compared with the $f_{\rm gas}$+CMB+SNIa results in Fig. 12 and 13, and in Table 3. The $f_{\rm gas}$+CMB+SNIa combination already provides tight constraints on $\Omega_{\rm m}$, h, $\Omega_{\rm b}h^2$ and n_s, but the degeneracy between w and σ_8 (Fig. 12) limits the precision of the dark energy results. The addition of the XLF data breaks the degeneracy in the $\Omega_{\rm m}$-σ_8 plane (Fig. 13), resulting in tighter constraints on $\Omega_{\rm m}$, σ_8 and w (Table 3).

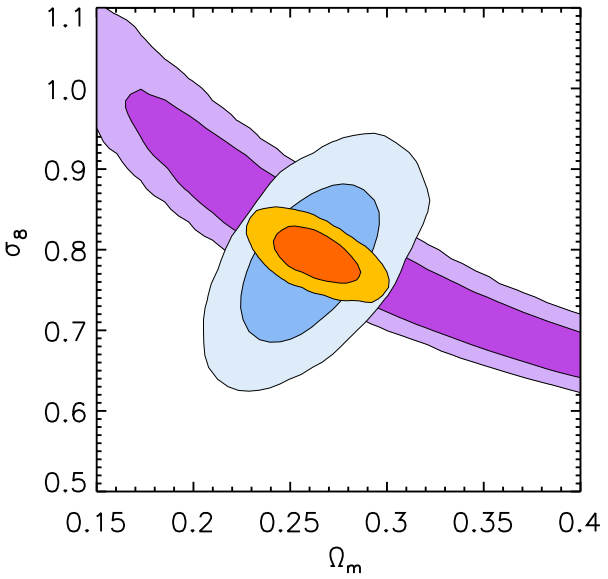

Figure 13. The joint constraints (68.3 and 95.4 per cent confidence) for a wCDM model on Ω_m and σ_8 obtained from a combined SNIa+f_{gas}+CMB analysis (blue) are compared with the constraints from the XLF alone (purple, marginalized over n_s). The results from combining all four data sets using importance sampling are shown in gold. No priors on h, $\Omega_b h^2$ or n_s are imposed. This figure demonstrates the degeneracy breaking power available from the combination of the data sets.

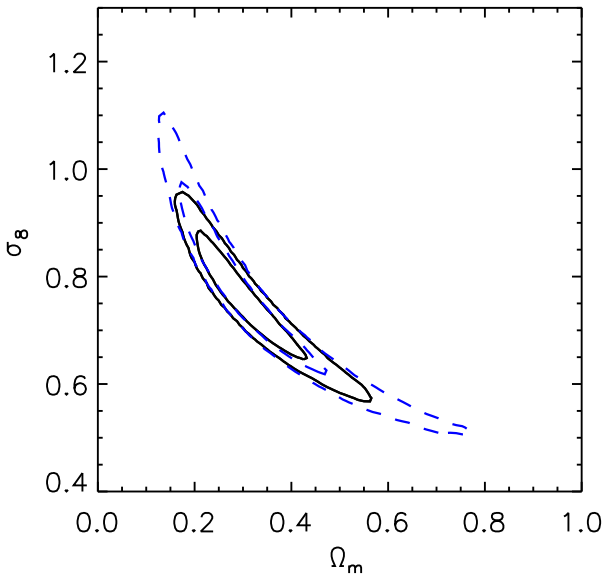

Figure 14. Comparison of joint 68.3 and 95.4 per cent confidence constraints on Ω_m and σ_8 for a constant-w model using standard priors (solid, black lines) and weak priors on h and $\Omega_b h^2$ (dashed, blue lines). Weakening these priors results in an expansion of the confidence region along the Ω_m-σ_8 degeneracy axis. The constraint on w is essentially unaffected (Table 2).

Table 3. Best-fitting values and marginalized 68.3 per cent confidence limits on cosmological parameters obtained from a combined analysis of the f_{gas}+CMB+SNIa data, and the combination of those results with the X-ray luminosity function (XLF) data by importance sampling. No priors on h, $\Omega_b h^2$ or n_s are used in either analysis.

	f_{gas}+CMB +SNIa	XLF+f_{gas} +CMB+SNIa
Ω_m	0.258 ± 0.022	0.263 ± 0.014
σ_8	0.79 ± 0.06	0.79 ± 0.02
w	-0.99 ± 0.07	-1.00 ± 0.05

6 DISCUSSION

6.1 Sensitivity to priors

In order to assess the sensitivity of these results to our standard priors, we have also performed analyses using the priors labeled as "weak" in Table 1: doubling the uncertainty on the mass function normalization, A, tripling the width of the Gaussian priors on h and $\Omega_b h^2$, and doubling the size of the allowed region for the mass–luminosity evolution parameter, γ. We will discuss the effect of these changes separately, having confirmed that they act independently.

A comparison of the results for prior sets 1, 4 and 5 in Table 2 demonstrates that marginalization over our standard and weak priors on A does not have a significant effect on the results. We therefore leave A fixed when producing the results shown in the remainder of Section 6.

Fig. 14 compares the constraints on Ω_m and σ_8 for a wCDM model using the standard and weak priors on h and $\Omega_b h^2$. Similar to the marginalization over n_s, the effect is to compound the Ω_m-σ_8 degeneracy. The constraint on w is essentially unchanged, as can be seen in Table 2.

The effect of changing the allowed region for γ on the Ω_m-w constraint is shown in Fig. 15, where the results obtained by fixing $\gamma = 0$ are compared with those of our standard and weak priors on γ. (We do not show the effect on σ_8 because it is very small for the ΛCDM models and nonexistent for the wCDM model.) There is an evident degeneracy between γ and w, but the non-self-similar evolution parametrized by γ must be large in order to significantly affect the constraint. Observations have not yet determined conclusively whether there is any departure from self-similar evolution in the mass–luminosity relation; some studies have claimed significant detections (Vikhlinin et al. 2002; Maughan 2007), while others have not (Maughan et al. 2006; Morandi et al. 2007). The most recent report of detection (Maughan 2007) corresponds to a shift in normalization of about 10 per cent by redshift 0.7, which is covered by our standard prior on γ. We note, however, that none of these analyses address the effects of data collection (e.g. Malmquist bias) which, if present, will tend to produce a spuriously strong signal of evolution with redshift.

6.2 AGN contamination

The presence of active galactic nuclei (AGN) and other point-like X-ray emitters is a potential concern for the accuracy of the mass–luminosity relation. There is no possibility of subtracting these point sources from the RASS data, since the number of photons in a cluster detection is typically too small. However, they are subtracted from the RB02 luminosities, to the extent that *ROSAT* can resolve them. In addition, there is the possibility of an increase in

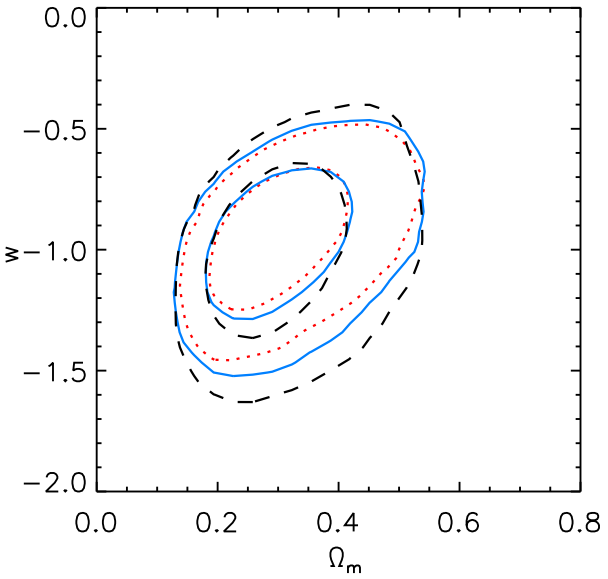

Figure 15. Comparison of joint 68.3 and 95.4 per cent confidence constraints on $\Omega_{\rm m}$ and w for a constant-w model assuming strictly self-similar evolution of the mass–luminosity relation ($\gamma = 0$; dotted, red lines) and using our standard (solid, blue lines) and weak (dashed, black lines) prior on γ. A weak degeneracy between γ and w is evident; doubling the width of the γ prior expands the w constraint by only 15 per cent.

the density of AGN over the redshift range of our data (e.g. Hasinger, Miyaji, & Schmidt 2005 and references therein). There may therefore be a mismatch between luminosities inferred from the RASS data and those used in the calibration of the mass–luminosity relation. In our work studying MACS clusters (in preparation), we take advantage of the *Chandra* X-ray Observatory's high spatial resolution to efficiently identify point sources and determine their contribution to the total cluster luminosity. We find that this contribution is at the per cent level – much smaller than the typical survey flux uncertainty – which indicates that point source contamination is not an issue for the current study.

6.3 Intrinsic and measurement luminosity scatter

The mass distribution of clusters available to a flux-limited survey is influenced by the degree of scatter in flux for a given mass. As described previously, this effect can be decomposed into a convolution of intrinsic scatter in the mass–luminosity relation and measurement error in the survey flux determinations. Failure to account for either of these sources of scatter when evaluating the number of detectable clusters predicted by a set of model parameters can significantly bias the result. The magnitude of the effect is demonstrated in Fig. 16, which shows the constraints on $\Omega_{\rm m}$ and σ_8 for a wCDM cosmology obtained by ignoring either of these scatters individually. In each case, the results are biased towards lower $\Omega_{\rm m}$ and higher σ_8, parallel to the degeneracy between the two parameters. The bias is small when ignoring the measurement scatter, but ignoring the intrinsic dispersion results in a significant bias. As can be seen in Table 2, the constraint on w is not significantly affected in either case. We note that these comments regarding the intrinsic dispersion apply equally well to mis-estimation of the uncertainty in the mass bias correction applied in Section 3.1.1; changing this quantity alters the error bars on the corrected masses, which directly affect the estimation of the intrinsic dispersion through Equation 11.

6.4 Bias in mass measurements

Any bias in the measured masses of the mass–luminosity data is completely degenerate with the normalization, α, which in turn affects inferences made on the other parameters. Fig. 17 (left panel) compares our constraints on $\Omega_{\rm m}$ and σ_8 to those that would be obtained without the correction to these masses motivated by departures from hydrostatic equilibrium, as described in Section 3.1.1. The fit in the latter case is biased towards significantly lower values of σ_8, such that the two of results are barely consistent at the 95.4 per cent confidence level. Importantly, however, the right panel of Fig. 17 demonstrates that the constraint on w is not significantly affected.

7 CONCLUSION

We have presented new constraints on cosmological constant (ΛCDM) and constant-w (wCDM) dark energy models using the observed X-ray luminosity function of the largest, most X-ray luminous galaxy clusters out to redshift 0.7, in combination with standard priors on h and $\Omega_{\rm b}h^2$. At 68.3 per cent confidence, we find $\Omega_{\rm m} = 0.27^{+0.06}_{-0.05}$ and $\sigma_8 = 0.77^{+0.07}_{-0.06}$ for a ΛCDM model, and $\Omega_{\rm m} = 0.28^{+0.08}_{-0.06}$, $\sigma_8 = 0.75 \pm 0.08$ and $w = -0.97^{+0.20}_{-0.19}$ for a wCDM model. These results include marginalization over uncertainties in the theoretical mass function and in non-self-similar evolution in the mass–luminosity relation, but not the spectral index. Marginalizing also over a conservative range of values of the spectral index, using no additional data, we still find $w = -0.96 \pm 0.21$. Our results constitute the first precise determination of the dark energy equation of state using measurements of the growth of cosmic structure observed in galaxy clusters, and provide a strong, independent confirmation of the validity of the cosmological constant model. The dark energy constraints are remarkably insensitive to the choice of priors and to the remaining systematic uncertainties in the analysis.

These results build upon, and are largely in agreement with, a number of earlier galaxy cluster studies (see Section 1). Our constraints on cosmological parameters are both consistent with and competitive with independent findings from studies of type Ia supernovae, anisotropies in the CMB, the X-ray gas mass fraction of galaxy clusters, galaxy redshift surveys and leading cosmic shear surveys. The agreement between the results from these independent techniques is reassuring, and motivates a combined analysis of the data in order to investigate more complex models of dark energy. We will pursue this strategy in future work. The preliminary combination through importance sampling presented in this paper indicates that significantly improved constraints on σ_8 and w can be obtained by combining the our data with CMB, SNIa and $f_{\rm gas}$ data; we find $\Omega_{\rm m} = 0.263 \pm 0.014$, $\sigma_8 = 0.79 \pm 0.02$ and $w = -1.00 \pm 0.05$.

The results for σ_8 presented here are somewhat higher

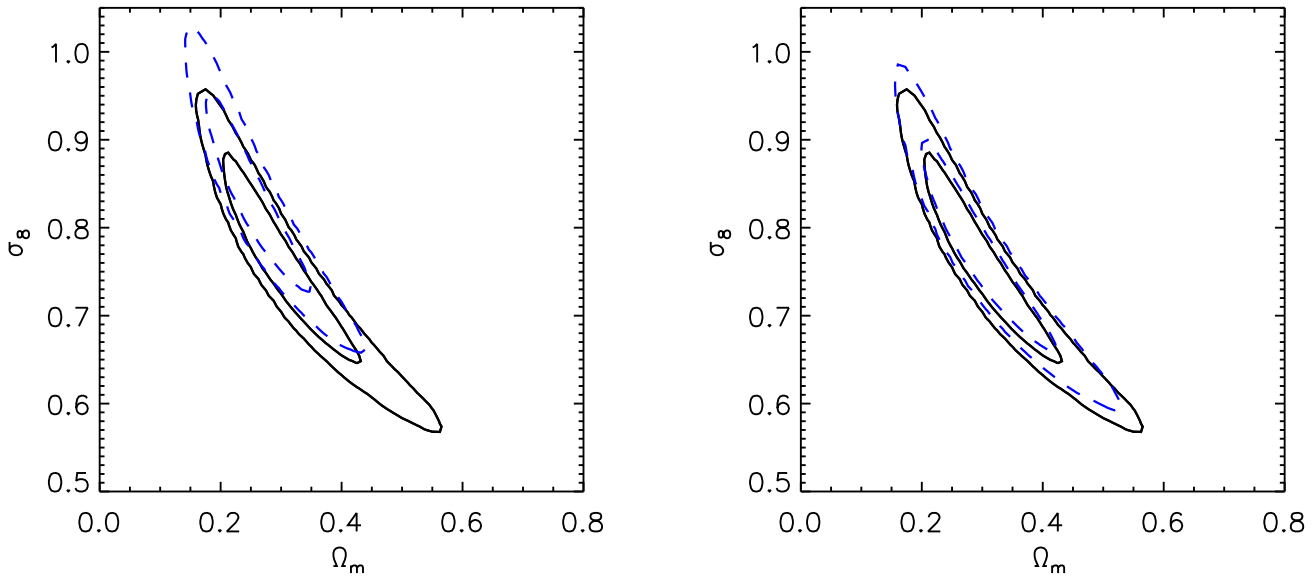

Figure 16. Comparison of joint 68.3 and 95.4 per cent confidence constraints on $\Omega_{\rm m}$ and σ_8 for a constant-w model using standard priors (solid, black lines) and results obtained by ignoring each source of luminosity scatter individually (dashed, blue lines). Left panel: the mass–luminosity intrinsic dispersion is fixed at $\eta = 0.0$. Right panel: measurement errors on survey luminosities are set to zero. Failing to account for the intrinsic dispersion in the mass–luminosity relation produces a significant bias towards higher values of σ_8 and lower values of $\Omega_{\rm m}$; a similar, but much smaller, bias is evident when the survey measurement error is not accounted for.

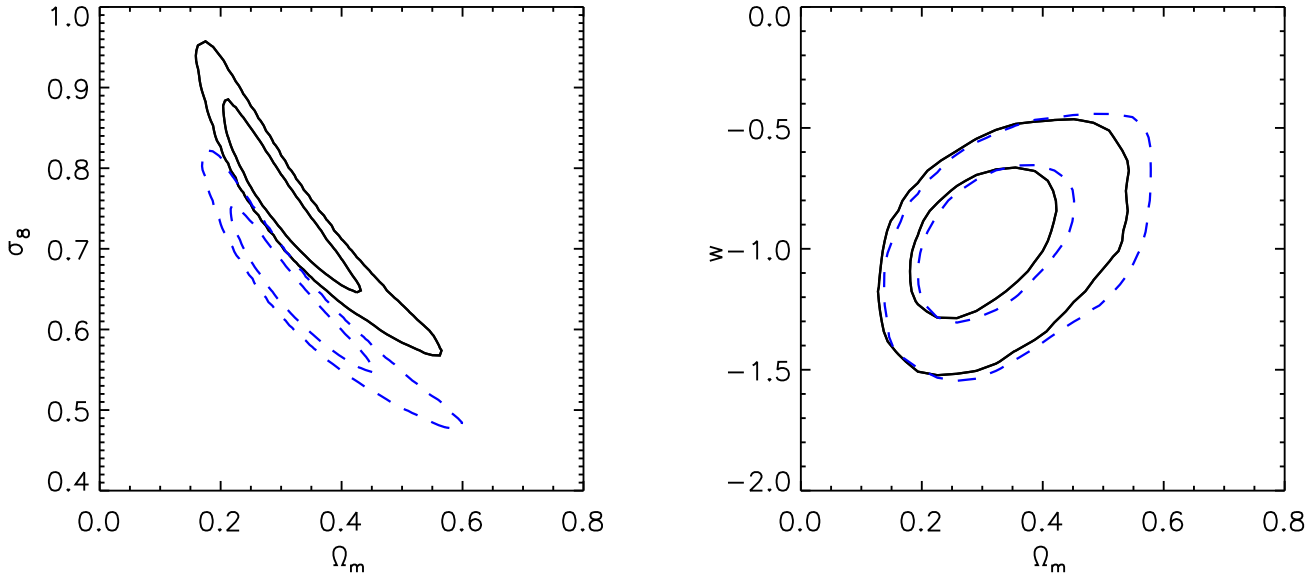

Figure 17. Comparison of joint 68.3 and 95.4 per cent confidence constraints for a constant-w model using standard priors (solid, black lines) and results obtained without correcting the RB02 masses for bias due to the assumption of hydrostatic equilibrium (Section 3.1.1; dashed, blue lines). Whereas the result for σ_8 is sensitive to the correction for non-thermal pressure support (left panel), the constraints on w (right panel) and $\Omega_{\rm m}$ are essentially independent.

than those from previous work based on the BCS and REFLEX data due to our correction to the masses used to constrain the mass–luminosity relation. The magnitude of this discrepancy underscores the need for an improved understanding of the X-ray observational biases resulting from asphericity, projection effects and hydrostatic disequilibrium. More advanced and comprehensive simulations, calibrated by gravitational lensing studies, show considerable promise in this area. Broad-band, high spectral resolution X-ray data from, for example, the New X-ray Telescope (NeXT) and Constellation-X, will allow precise measurements of gas velocities and non-thermal emission components in clusters, providing a more comprehensive understanding of the relevant gas physics.

Remaining systematics in the analysis appear to be relatively minor. In particular, uncertainty in the theoretical mass function and the redshift evolution of the scaling relation have a small effect on our results. However, we note

that the extension of this analysis to future, high-redshift X-ray (e.g. Spectrum-RG/eROSITA) or Sunyaev-Z'eldovich surveys will necessitate more rigorous study of galaxy cluster virial relations and their evolution, taking full account of selection effects.

ACKNOWLEDGMENTS

We thank Adrian Jenkins for providing computer code to evaluate the mass function of dark matter halos and Gil Holder for a helpful discussion. We also thank Glenn Morris and Stuart Marshall for computer support. Calculations for this work were carried out using the KIPAC XOC and Orange compute clusters at the Stanford Linear Accelerator Center (SLAC) and the SLAC Unix compute farm. We acknowledge support from the National Aeronautics and Space Administration through Chandra Award Numbers DD5-6031X, GO2-3168X, GO2-3157X, GO3-4164X and GO3-4157X, issued by the Chandra X-ray Observatory Center, which is operated by the Smithsonian Astrophysical Observatory for and on behalf of the National Aeronautics and Space Administration under contract NAS8-03060. This work was supported in part by the U.S. Department of Energy under contract number DE-AC02-76SF00515. AM was additionally supported in part by a Stanford Graduate Fellowship.

REFERENCES

Akritas M. G., Bershady M. A., 1996, ApJ, 470, 706
Allen S. W., Rapetti D. A., Schmidt R. W., Ebeling H., Morris G., Fabian A. C., 2007, MNRAS, submitted (astro-ph/07060033)
Allen S. W., Schmidt R. W., Fabian A. C., Ebeling H., 2003, MNRAS, 342, 287
Astier P. et al., 2006, A&A, 447, 31
Benjamin J. et al., 2007, MNRAS, in press (astro-ph/0703570)
Böhringer H. et al., 2004, A&A, 425, 367
Böhringer H. et al., 2001, A&A, 369, 826
Böhringer H. et al., 2000, ApJS, 129, 435
Borgani S. et al., 2001, ApJ, 561, 13
Bryan G. L., Norman M. L., 1998, ApJ, 495, 80
Cavaliere A., Fusco-Femiano R., 1978, A&A, 70, 677
Cole S. et al., 2005, MNRAS, 362, 505
Dahle H., 2006, ApJ, 653, 954
Davis T. M. et al., 2007, ApJ, in press (astro-ph/0701510)
Donahue M., Voit G. M., 1999, ApJL, 523, L137
Ebeling H., 1993, Ph.D. thesis, Ludwig Maximilians Universitat Munich, (1993)
Ebeling H., Barrett E., Donovan D., Ma C.-J., Edge A. C., van Speybroeck L., 2007, ApJL, 661, L33
Ebeling H., Edge A. C., Allen S. W., Crawford C. S., Fabian A. C., Huchra J. P., 2000, MNRAS, 318, 333
Ebeling H., Edge A. C., Bohringer H., Allen S. W., Crawford C. S., Fabian A. C., Voges W., Huchra J. P., 1998, MNRAS, 301, 881
Ebeling H., Edge A. C., Henry J. P., 2001, ApJ, 553, 668
Ebeling H., Wiedenmann G., 1993, Phys. Rev. E, 47, 704
Eisenstein D. J., Hu W., 1998, ApJ, 496, 605
Eisenstein D. J. et al., 2005, ApJ, 633, 560
Eke V. R., Baugh C. M., Cole S., Frenk C. S., Navarro J. F., 2006, MNRAS, 370, 1147
Eke V. R., Cole S., Frenk C. S., Patrick Henry J., 1998, MNRAS, 298, 1145
Evrard A. E. et al., 2002, ApJ, 573, 7
Faltenbacher A., Kravtsov A. V., Nagai D., Gottlöber S., 2005, MNRAS, 358, 139
Freedman W. L. et al., 2001, ApJ, 553, 47
Gelman A., Rubin D. B., 1992, Statis. Sci., 7, 457
Haiman Z., Mohr J. J., Holder G. P., 2001, ApJ, 553, 545
Hasinger G., Miyaji T., Schmidt M., 2005, A&A, 441, 417
Henry J. P., 2000, ApJ, 534, 565
Henry J. P., 2004, ApJ, 609, 603
Hu W., Kravtsov A. V., 2003, ApJ, 584, 702
Jenkins A., Frenk C. S., White S. D. M., Colberg J. M., Cole S., Evrard A. E., Couchman H. M. P., Yoshida N., 2001, MNRAS, 321, 372
Jha S., Riess A. G., Kirshner R. P., 2007, ApJ, 659, 122
Klypin A., Macciò A. V., Mainini R., Bonometto S. A., 2003, ApJ, 599, 31
Kravtsov A. V., Vikhlinin A., Nagai D., 2006, ApJ, 650, 128
Levine E. S., Schulz A. E., White M., 2002, ApJ, 577, 569
Lewis A., Bridle S., 2002, Phys. Rev. D, 66, 103511
Linder E. V., 2005, Phys. Rev. D, 72, 043529
Linder E. V., Jenkins A., 2003, MNRAS, 346, 573
Łokas E. L., Bode P., Hoffman Y., 2004, MNRAS, 349, 595
Majumdar S., Mohr J. J., 2003, ApJ, 585, 603
Majumdar S., Mohr J. J., 2004, ApJ, 613, 41
Massey R. et al., 2007, ApJS, in press (astro-ph/0701480)
Maughan B. J., 2007, ApJ, in press (astro-ph/0703504)
Maughan B. J., Jones L. R., Ebeling H., Scharf C., 2006, MNRAS, 365, 509
Miknaitis G. et al., 2007, ApJ, submitted (astro-ph/0701043)
Morandi A., Ettori S., Moscardini L., 2007, MNRAS, 379, 518
Nagai D., Vikhlinin A., Kravtsov A. V., 2007, ApJ, 655, 98
Navarro J. F., Frenk C. S., White S. D. M., 1997, ApJ, 490, 493
O'Meara J. M., Tytler D., Kirkman D., Suzuki N., Prochaska J. X., Lubin D., Wolfe A. M., 2001, ApJ, 552, 718
Percival W. J. et al., 2007, ApJ, 657, 51
Pierpaoli E., Borgani S., Scott D., White M., 2003, MNRAS, 342, 163
Rapetti D., Allen S. W., Amin M. A., Blandford R. D., 2007, MNRAS, 375, 1510
Rapetti D., Allen S. W., Weller J., 2005, MNRAS, 360, 555
Rasia E. et al., 2006, MNRAS, 369, 2013
Reiprich T. H., Böhringer H., 2002, ApJ, 567, 716
Riess A. G. et al., 2007, ApJ, 659, 98
Rozo E. et al., 2007, ApJ, submitted (astro-ph/0703571)
Schuecker P., Böhringer H., Collins C. A., Guzzo L., 2003, A&A, 398, 867
Schuecker P. et al., 2001, A&A, 368, 86
Seljak U., 2002, MNRAS, 337, 769
Spergel D. N. et al., 2007, ApJS, 170, 377
Tegmark M. et al., 2006, Phys. Rev. D, 74, 123507
Trümper J., 1993, Science, 260, 1769

Viana P. T. P., Nichol R. C., Liddle A. R., 2002, ApJL, 569, L75
Vikhlinin A., VanSpeybroeck L., Markevitch M., Forman W. R., Grego L., 2002, ApJL, 578, L107
Vikhlinin A. et al., 2003, ApJ, 590, 15
Voevodkin A., Vikhlinin A., 2004, ApJ, 601, 610
Weller J., Battye R. A., Kneissl R., 2002, Phys. Rev. Lett., 88, 231301
White M., 2002, ApJS, 143, 241
Wood-Vasey W. M. et al., 2007, ApJ, submitted (astro-ph/0701041)

This paper has been typeset from a TEX/ LATEX file prepared by the author.